HHS Public Access

Author manuscript

J Mater Chem B. Author manuscript; available in PMC 2018 October 16.

Published in final edited form as:

J Mater Chem B. 2016 ; 4(18): 3031–3036. doi:10.1039/C5TB02618K.

In vitro electrochemical characterization of polydopamine melanin as a tissue stimulating electrode material

Ik Soo Kwon[a], **Young Jo Kim**[a], **Luke Klosterman**[a], **Mats Forssell**[b], **Gary K. Fedder**[b,c], and **Christopher J. Bettinger**[a,d,e]

[a]Department of Materials Science and Engineering, Carnegie Mellon University 5000 Forbes Ave, Pittsburgh, PA 15213 (USA)

[b]Department of Electrical and Computer Engineering, Carnegie Mellon University 5000 Forbes Ave, Pittsburgh, PA 15213 (USA)

[c]The Robotics Institute, Carnegie Mellon University, 5000 Forbes Ave, Pittsburgh, PA 15213 (USA)

[d]Department of Biomedical Engineering, Carnegie Mellon University 5000 Forbes Ave, Pittsburgh, PA 15213 (USA)

[e]McGowan Institute for Regenerative Medicine, University of Pittsburgh 450 Technology Drive, Suite 300, Pittsburgh, PA 15219 (USA)

Abstract

The properties of redox active polydopamine melanin (PDM) films as a coating material for neural electrodes were evaluated. PDM films with nanometer-scale thicknesses exhibit dc bias dependent charge injection capacities (CIC) with maximum values of 110 ± 23 μC cm^{-2} at 0.2V (vs Ag/AgCl) and reduce the interfacial impedance compared to inorganic conducting films. PDM films exhibited an asymmetric impedance response to positive and negative dc biases with minimum interfacial impedance at 0.2V (vs Ag/AgCl). An explanation for the observed bias-dependent electrochemical behavior is presented.

Brain-machine interfaces are essential components in neuromodulation devices with prospective applications ranging from rehabilitation to therapeutic interventions.[1–7] Miniaturizing electrode geometries is essential for increasing the specificity and selectivity during recording and stimulation sequences. Microelectrodes with nominal surface areas smaller than 10,000 $μm^2$ are often used.[8–12] Arbitrarily reducing the electrode size increases the impedance and reduces the charge stimulation capacity.[9–13]

The charge injection capacity (CIC) is a key figure of merit to assess the performance of neural electrodes. The CIC can be improved by increasing roughness for given geometric surface area (GSA) or by utilizing coatings with improved electrochemical coupling.[8,14]

Correspondence to: Christopher J. Bettinger.

†Electronic Supplementary Information (ESI) available: Experimental Details and additional electrochemical data. See DOI: 10.1039/x0xx00000x

Faradaic charge injection mechanisms can increase CIC compared to capacitive double layer charging during stimulation.[8,11,15,16] However, next-generation materials to improve the performance of neural electrodes may present unknown risks including intrinsic cytotoxicity or injurious macroscopic tissue-materials interactions.[17–20] The majority of data sets regarding the toxicity and biocompatibility of conducting polymers such as polythiophenes and polyaniline have been generated using in vitro models, which only partially recapitulate in vivo behavior.[18] Translation of devices containing conducting polymers will require rigorous and long-term evaluation of safety and efficacy since many polymers and associated monomers present an unknown risk to prospective subjects. Polymers based on naturally occurring precursors could accelerate the timeline for clinical translation of next-generation materials to improve the performance of neural electrodes. Conjugated polymers from natural monomers that exhibit Faradaic reactions could improve charge injection and therefore support electrode miniaturization. Polydopamine melanin (PDM) is redox active conjugated polymer formed from oxidative polymerization of dopamine. Herein, we synthesized PDM films and evaluated the potential of this material as an electrode coating for prospective applications in neuromodulation.

Melanins are a broad class of pigments that exhibit unique physical properties such as efficient photon-phonon conversion and free radical scavenging.[21,22] Eumelanin, one of the most common types of natural melanin, and their synthetic analogues have been explored in the context of various applications due to their unique ionic and electronic properties.[23–29] Natural eumelanin is essentially an amorphous heterogeneous biopolymer composed primarily of random ensembles of 5,6-dihydroxyindole (DHI) and 5,6-dihydroxyindole-2-carboxylic acid (DHICA).[30–33] DHI/DHICA protomolecules stack randomly via **π-π** interactions and H-bonding to form heterogeneous aggregates.[34–47] Natural eumelanin also contains high densities of redox active catechol groups (~4.8×10^{21} #/cm^3) and exhibits hydration-dependent hybrid proton-electron conductivity.[38] Taken together, these properties suggest that melanin pigments may support Faradaic mechanisms that could increase the CIC. Polydopamine melanin (PDM) is a synthetic analogue of natural eumelanin that shares many physical properties of the former, and is a major component of naturally occurring melanin pigments found in the human body.[39,40] PDM exhibits robust redox activity, primarily through DHI subunits, that are leveraged in free radical scavenging.[30,39] PDM is electromechanically stable, can be formed through facile synthetic routes, and exhibits satisfactory adhesion to diverse substrate materials.[40–48] PDM films were chosen as the synthetic melanin composition for further study.

PDM films were deposited through auto-oxidative polymerization of dopamine precursors in aqueous solutions.[44] Cleaned indium tin oxide substrates were placed in a stock solution of 2mg/ml dopamine hydrochloride in 50mM carbonate/bicarbonate buffer (pO_2 = 160 mmHg; 25 ± 3 °C; pH = 8.5). Deposition times of 16 hr produce PDM film with nominal thicknesses of 40nm. The CIC (Q_{inj}) of bare indium tin oxide (ITO) and PDM-coated ITO electrodes ([Area] = 1 cm^2) was compared using voltage transient measurements in 0.01M PBS solutions. Values for the RMS roughness of bare ITO and PDM-coated ITO electrodes were 2.42 ± 0.13 nm and 79.9 ± 8.7 nm respectively, as measured by atomic force microscopy (AFM) (Table S1.). Current pulses were delivered as cathodal-first, symmetric charge balanced biphasic pairs, since charge balanced (net overall zero charge) and cathodal-first

pulses are employed *in vivo* setting to avoid tissue and electrode damage.[8] An example of voltage transient responses of ITOs and PDM electrodes are shown in Fig. 1.

The parameter V_{bias} defines the potential of an electrode immediately before current is applied and because the decay time is much slower than the duration of the experiment, it is equivalent to dc bias of the sample (vs. Ag/AgCl reference electrodes). The value of V_a is the access voltage, which is the voltage drop associated with the ohmic components within the system such as solution and external circuit resistances and is assumed to be nearly instantaneous. A dwell time of 1ms was employed between the cathodic and anodic pulse to determine V_a.[8] The observed values for E_{mc} and E_{ma}, the most negative and positive polarization of an electrode, are given by the following relationships:

$$E_{mc} = V_{max-neg} - V_a$$

$$E_{ma} = V_{max-pos} - V_a$$

$V_{max\text{-}neg}$ ($V_{max\text{-}pos}$) is the maximum negative (positive) voltage transient. Current pulse-widths were fixed at 10ms and the current amplitude increased from low current amplitude until the values of E_{mc} or E_{ma} reach the limit of the water stability window (−0.6V to 0.8V vs. Ag/AgCl).[15,16,49,50] The values of Q_{inj} were calculated by multiplying the amplitude by the pulse width.

The values of Q_{inj} of ITO and PDM electrodes are plotted as a function of bias potential (V_{bias}) (Fig. 2). PDM electrodes exhibit a larger Q_{inj} compared to electrodes composed of bare ITO electrodes as observed in a six-fold increase in Q_{inj} at 0.2V bias versus Ag/AgCl. Values for $Q_{inj\text{-}PDM}$ exhibit a stronger bias dependency compared to $Q_{inj\text{-}ITO}$. Values of $Q_{inj\text{-}PDM}$ increase to 110 ± 23 μC cm^{-2} (n=3), which is comparable to that of Pt electrodes (50~150 μC cm^{-2})[50] and smaller than the CIC of activated iridium oxide (AIROF; 1–5 mC cm^{-2}) or poly(3,4-ethylenedioxythiophene) (PEDOT;15 mC cm^{-2}), two redox active materials that have been used extensively as coatings to improve the performance of both stimulating and recording electrodes.[8] Previously reported values of Q_{inj} of PEDOT are attributed to the large effective electrochemical surface area (ESA) that results from highly porous nanostructures.[11,51–54] Increased ratios of ESA to geometric surface area (GSA) are also responsible in part for large observed values of Q_{inj} in AIROF electrodes.[55] However, calculations based on AFM roughness using Gwyddion (See Supporting Information) suggests that there is only a 10% increase in the effective surface area with PDM coating compared to bare ITO. Thus, the observed increase in CIC with PDM coating is a result of the intrinsic electrochemical nature of PDM as opposed to extrinsic geometric factors associated with the morphology of PDMS thin films.

The prospective mechanisms for charge injection were investigated sugin electrochemical impedance spectroscopy (EIS) was used for the mechanistic study. The EIS responses of substrates composed of either bare ITO or ITO with a PDM film 40nm in thickness at open circuit potential are shown in Fig. 3. A Nyquist plot (Fig. 3a) shows that films composed of

bare ITO display a typical near vertical capacitive line, while the PDM film's response deviates from the capacitive line. In the high frequency region (f>1kHz), the impedance responses of both ITO and PDM electrodes are largely governed by frequency independent ohmic components such as external circuit and solution resistance in the system. These conclusions are supported by a plateau region in the plot of modulus versus frequency and near 0° phase in the phase plot (Fig. 3b and c).[46,57] However, for f < 100Hz, ohmic components that are insensitive to frequency are suppressed, the interfacial impedance dominates the response of the system, and the reduction of interfacial impedance in electrodes with PDM thin films is observed (Fig. 2b).

A phase angle of $\theta \sim 90°$ at low frequencies (f < 100Hz) for bare ITO electrodes indicates ion and electron blocking behaviour of this material where negligible Faradaic reactions take place. Capacitive double layer formation is therefore the dominant mechanism for charging the electrode.[57] Wünsche et al. posited that charge transfer at the electrode/PDM interface governs the impedance response of PDM films at dc biases >0.2V (vs. Ag/AgCl). Furthermore, the PDM film response exhibits blocking behavior in the absence of dc bias.[58] However, the constant rise in phase angle from f=10Hz to f=0.1Hz for thin film PDM electrodes (Fig. 3c) suggests that the impact of parallel redox reactions is subtle compared to the anticipated response from the ideal Randles circuit.[56,57,59,60]

EIS data were conducted for both bare ITO and PDM electrodes (40nm in thickness) various dc biases from −0.6V to 0.6V versus Ag/AgCl. The response of bare ITO electrodes was largely capacitive except for strongly negative biases (<−0.4V). Here the response is likely to be attributed to H^+ reduction (Fig. S4). Electrodes coated with PDM films 40nm in thickness exhibit a strong voltage dependence (Fig. 4). As the dc bias is reduced (more negative), the characteristic semicircle behaviour in $-Z''$ versus Z' becomes more evident. These data suggest that redox activity becomes more prominent and the charge transfer R_{ct} is reduced as the dc bias becomes more negative.[56] However, for the case of positive biases, the opposite trend is true. A linear relationship between $-Z''$ and Z' with a slope of unity is observed for a bias of 0.2V. Bode plots indicate that bias-dependent interfacial impedance is smallest at 0.2V for PDM. These data are consistent with CIC data in which the maximum observed values for CIC occur at 0.2V (Fig. S5). Plots of $-Z''$ vs. Z' exhibit a semicircle shape for dc biases of 0.4V and 0.6V (larger radius and therefore larger R_{ct} for 0.6V). The linear region of $-Z''$ vs. Z' indicates a possible transition to a mass-transfer regime.

UV-vis absorption spectra of PDM films were largely consistent as a function of applied dc biase (Fig. S6). The asymmetric electrochemical behaviour of PDM films with respect to applied dc bias voltage could be explained by considering the interplay between the redox active moieties in PDM and hydrogen reduction in aqueous environments. Wünsche et al. suggested that with full reduction and oxidation of PDM, formation of hydroquinone (H_2Q) at the negatively biased PDM/substrate interface and formation of quinone imine (QI^-) at the positively biased PDM/substrate interface decreases electronic current in PDM.[58] Similar phenomena may be considered in the present system. For PDM films under positive dc bias, increased formation of QI^- at the PDM/ITO interface with increasing polarization could decrease the electronic current and in turn, increase the observed values of R_{ct}. EIS data recorded for bare ITO electrodes suggests that proton reduction becomes more prominent as

the magnitude of the dc bias is increased (negative overall bias) (Fig. S4). H_2Q formation could increase R_{ct} as the overall dc bias becomes more negative. However, the active reduction of protons with increasingly negative bias serves as a pathway for electrons to leave the PDM film thereby preventing H_2Q formation at the PDM/ITO interface. Attenuated formation of fully reduced H_2Q therefore decreases the expected value for R_{ct}.

The thickness-dependent impedance responses for PDM electrodes were recorded for 40nm, 80nm, and 120nm films at biases of 0.6V and −0.6V versus Ag/AgCl (Fig. 5a). EIS data was fit to an equivalent circuit to extract the values of R_{ct} as a function of film thickness (Fig. 5c). The exact fitting of EIS data of electrodes composed of PDM films on ITO substrates requires a complex model that accounts for mixed electronic-ionic conductivity in PDM and proton reduction under negative dc bias.[59,61,62] The intrinsic chemical heterogeneity of PDM in these films present unique challenges in fitting an appropriate model for the low frequency regime (f<1Hz). The low frequency regime is mass transfer limited and therefore inextricably linked to the chemistry and complex nanostructure of the film.[63] Since the focus is dedicated to understanding the evolution of R_{ct}, data was fit by focusing on the f>1Hz region (kinetic region) (Fig. 5c). A Randles circuit without Warburg impedance (excluding the mass transfer limited regime) serves as a suitable description for the frequency response of PDM films for f>1Hz (Fig. 5c). A parallel RC element was added in series with the double layer capacitance to account for non-negligible film resistance and thickness-dependent capacitance at high frequencies.[64] Calculated values of R_{ct} are shown in Fig. 5d. Biases of 0.6V (−0.6V) decrease (increase) the extracted values of R_{ct} with increasing PDM film thickness.

Extracted values for R_{ct} are inversely proportional to the thickness of PDM films biased at 0.6V. This trend is also observed in IrOx and is attributed to increased redox active sites in films.[8,65] At a bias of −0.6V, H^+ reduction decreases with increasing thickness, a phenomenon that is attributed to increased observed values of R_{ct} versus PDM film thickness. As the distance between PDM/solution interface and PDM/electrode interface increases, incomplete H^+ reduction limits H_2Q formation thereby increasing observed values for R_{ct}.

The charge injection capacity of PDM was calculated to be 110 ± 23 μC cm^{-2}, a significant increase compared to bare ITO. AFM data suggest that increasing the ratio of ESA:GSA could further increase the CIC. Redox activity in PDM and reduced interfacial impedance for PDM (compared to bare ITO) was observed by EIS. The asymmetric behaviour of PDM film to dc bias is attributed to full oxidation/reduction of PDMs along with H^+ reduction. Limiting the extent of fully oxidized and reduced films could increase the performance of PDM as a coating material for implantable electrodes. Future studies will validate the proposed mechanism through systematic CV and other electrochemical methods. Prospective non-conventional processing techniques are also envisioned to increase the ratio of ESA:GSA.

Supplementary Material

Refer to Web version on PubMed Central for supplementary material.

Acknowledgments

The authors acknowledge the financial support provided by the following organizations: American Chemical Society (PRF51980DN17); the Carnegie Mellon University (CMU) School of Engineering; the Pennsylvania Department of Community and Economic Development; Innovation Works (Pittsburgh, PA); the Department of Energy (DE-OE000226); the CMU Center for Technology Transfer and Enterprise Creation; the Shurl and Kay Curci Foundation; Defense Advanced Research Projects Agency (D14AP00040); National Institues of Health (R21NS095250); National Science Foundation (DMR1542196).

References

1. Carmena JM, Lebedev MA, Crist RE, O'Doherty JE, Santucci DM, Dimitrov DF, Patil PG, Henriquez CS, Nicolelis MAL. Plos Biol. 2003; 1:193–208.
2. Dobelle WH. Asaio J. 2000; 46:3–9. [PubMed: 10667705]
3. Donoghue JP. Nat Neurosci. 2002; 5:1085–1088. [PubMed: 12403992]
4. Kennedy PR, Bakay RAE. Neuroreport. 1998; 9:1707–1711. [PubMed: 9665587]
5. Nicolelis MAL. Nat Rev Neurosci. 2003; 4:417–422. [PubMed: 12728268]
6. Salinas E, Abbott LF. J Comput Neurosci. 1994; 1:89–107. [PubMed: 8792227]
7. Serruya MD, Hatsopoulos NG, Paninski L, Fellows MR, Donoghue JP. Nature. 2002; 416:141–142. [PubMed: 11894084]
8. Cogan SF. Annu Rev Biomed Eng. 2008; 10:275–309. [PubMed: 18429704]
9. Drake KL, Wise KD, Farraye J, Anderson DJ, Bement SL. Ieee T Bio-Med Eng. 1988; 35:719–732.
10. Humphrey D, Schmidt E. Neurophysiological Techniques. Boulton A, Baker G, Vanderwolf C, editorsVol. 15. Humana Press; 1990. 1–64.
11. Ludwig KA, Uram JD, Yang JY, Martin DC, Kipke DR. J Neural Eng. 2006; 3:59–70. [PubMed: 16510943]
12. Paik SJ, Park Y, Cho DI. J Micromech Microeng. 2003; 13:373–379.
13. Robinson DA. Proceedings of the IEEE. 1968; 56:1065–1071.
14. Weiland JD, Anderson DJ, Humayun MS. IEEE Trans Biomed Eng. 2002; 49:1574–1579. [PubMed: 12549739]
15. Beebe X, Rose TL. Ieee T Bio-Med Eng. 1988; 35:494–495.
16. Cogan SF, Troyk PR, Ehrlich J, Plante TD, Detlefsen DE. Ieee T Bio-Med Eng. 2006; 53:327–332.
17. Cogan SF, Guzelian AA, Agnew WF, Yuen TGH, McCreery DB. J Neurosci Meth. 2004; 137:141–150.
18. Green RA, Lovell NH, Wallace GG, Poole-Warren LA. Biomaterials. 2008; 29:3393–3399.
19. McCreery DB, Agnew WF, Bullara LA. Ann Biomed Eng. 2002; 30:107–119. [PubMed: 11874134]
20. Rosenber B, Vancamp L, Krigas T. Nature. 1965; 205:698-&. [PubMed: 14287410]
21. Riley PA. Int J Biochem Cell B. 1997; 29:1235–1239.
22. Prota G. Melanins and Melanogenesis. Academic Press; New York: 1992.
23. Ambrico M, Ambrico PF, Cardone A, Della Vecchia NF, Ligonzo T, Cicco SR, Talamo MM, Napolitano A, Augelli V, Farinola GM, d'Ischia M. J Mater Chem C. 2013; 1:1018–1028.
24. Ambrico M, Cardone A, Ligonzo T, Augelli V, Ambrico PF, Cicco S, Farinola GM, Filannino M, Perna G, Capozzi V. Org Electron. 2010; 11:1809–1814.
25. Ambrico M, Ambrico PF, Cardone A, Ligonzo T, Cicco SR, Di Mundo R, Augelli V, Farinola GM. Adv Mater. 2011; 23:3332-+. [PubMed: 21671448]
26. Ambrico M, Ambrico PF, Cardone A, Cicco SR, Palumbo F, Ligonzo T, Di Mundo R, Petta V, Augelli V, Favia P, Farinola GM. J Mater Chem C. 2014; 2:573–582.
27. Capozzi V, Perna G, Carmone P, Gallone A, Lastella M, Mezzenga E, Quartucci G, Ambrico M, Augelli V, Biagi PF, Ligonzo T, Minafra A, Schiavulli L, Pallara M, Cicero R. Thin Solid Films. 2006; 511:362–366.
28. Wunsche J, Cicoira F, Graeff CFO, Santato C. J Mater Chem B. 2013; 1:3836–3842.

29. Wunsche J, Cardenas L, Rosei F, Cicoira F, Gauvin R, Graeff CFO, Poulin S, Pezzella A, Santato C. Adv Funct Mater. 2013; 23:5591–5598.
30. d'Ischia M, Wakamatsu K, Napolitano A, Briganti S, Garcia-Borron JC, Kovacs D, Meredith P, Pezzella A, Picardo M, Sarna T, Simon JD, Ito S. Pigm Cell Melanoma R. 2013; 26:616–633.
31. Gidanian S, Farmer PJ. J Inorg Biochem. 2002; 89:54–60. [PubMed: 11931963]
32. Meredith P, Sarna T. Pigm Cell Res. 2006; 19:572–594.
33. Pezzella A, Iadonisi A, Valerio S, Panzella L, Napolitano A, Adinolfi M, d'Ischia M. J Am Chem Soc. 2009; 131:15270–15275. [PubMed: 19919162]
34. Pezzella A, Wünsche J. Organic Electronics: Emerging Concepts and Technologies. Wiley-VCH Verlag GmbH & Co; KGaA, Weinheim, Germany: 2013.
35. Arzillo M, Mangiapia G, Pezzella A, Heenan RK, Radulescu A, Paduano L, d'Ischia M. Biomacromolecules. 2012; 13:2379–2390. [PubMed: 22651227]
36. Clancy CMR, Simon JD. Biochemistry-Us. 2001; 40:13353–13360.
37. Watt AAR, Bothma JP, Meredith P. Soft Matter. 2009; 5:3754–3760.
38. Mostert AB, Powell BJ, Pratt FL, Hanson GR, Sarna T, Gentle IR, Meredith P. P Natl Acad Sci USA. 2012; 109:8943–8947.
39. d'Ischia M, Napolitano A, Ball V, Chen CT, Buehler MJ. Accounts Chem Res. 2014; 47:3541–3550.
40. Liu YL, Ai KL, Lu LH. Chem Rev. 2014; 114:5057–5115. [PubMed: 24517847]
41. Fei B, Qian BT, Yang ZY, Wang RH, Liu WC, Mak CL, Xin JH. Carbon. 2008; 46:1795–1797.
42. Ku SH, Lee JS, Park CB. Langmuir. 2010; 26:15104–15108. [PubMed: 20806924]
43. Ku SH, Park CB. Biomaterials. 2010; 31:9431–9437. [PubMed: 20880578]
44. Lee H, Dellatore SM, Miller WM, Messersmith PB. Science. 2007; 318:426–430. [PubMed: 17947576]
45. Lee H, Rho J, Messersmith PB. Adv Mater. 2009; 21:431-+. [PubMed: 19802352]
46. Lynge ME, van der Westen R, Postma A, Stadler B. Nanoscale. 2011; 3:4916–4928. [PubMed: 22024699]
47. Mrowczynski R, Turcu R, Leostean C, Scheidt HA, Liebscher J. Mater Chem Phys. 2013; 138:295–302.
48. Zhu LP, Yu JZ, Xu YY, Xi ZY, Zhu BK. Colloid Surface B. 2009; 69:152–155.
49. Cogan SF, Plante TD, Ehrlich J. 2004
50. Rose TL, Robblee LS. Biomedical Engineering, IEEE Transactions on. 1990; 37:1118–1120.
51. Richardson-Burns SM, Hendricks JL, Foster B, Povlich LK, Kim DH, Martin DC. Biomaterials. 2007; 28:1539–1552. [PubMed: 17169420]
52. Yang JY, Kim DH, Hendricks JL, Leach M, Northey R, Martin DC. Acta Biomater. 2005; 1:125–136. [PubMed: 16701786]
53. Bobacka J, Lewenstam A, Ivaska A. J Electroanal Chem. 2000; 489:17–27.
54. Cui XY, Martin DC. Sensor Actuat B-Chem. 2003; 89:92–102.
55. Lu Y, Cai ZX, Cao YL, Yang HX, Duan YY. Electrochem Commun. 2008; 10:778–782.
56. Macdonald JR, Barsoukov E. History. 2005; 1:8.
57. Orazem ME, Tribollet B. Electrochemical impedance spectroscopy. John Wiley & Sons; 2011.
58. Wunsche J, Deng YX, Kumar P, Di Mauro E, Josberger E, Sayago J, Pezzella A, Soavi F, Cicoira F, Rolandi M, Santato C. Chem Mater. 2015; 27:436–442.
59. Ho C, Raistrick ID, Huggins RA. J Electrochem Soc. 1980; 127:343–350.
60. Franceschetti DR, Macdonald JR. Small-signal AC response theory for electrochromic thin films. Defense Technical Information Center; 1981.
61. Vorotyntsev MA. Electrochim Acta. 2002; 47:2071–2079.
62. Vorotyntsev MA, Deslouis C, Musiani MM, Tribollet B, Aoki K. Electrochim Acta. 1999; 44:2105–2115.
63. Inzelt G, Láng GG. Electropolymerization: Concepts, Materials and Applications. 2010:51–76.
64. Freger V, Bason S. J Membrane Sci. 2007; 302:1–9.

65. Slavcheva E, Vitushinsky R, Mokwa W, Schnakenberg U. J Electrochem Soc. 2004; 151:E226–E237.

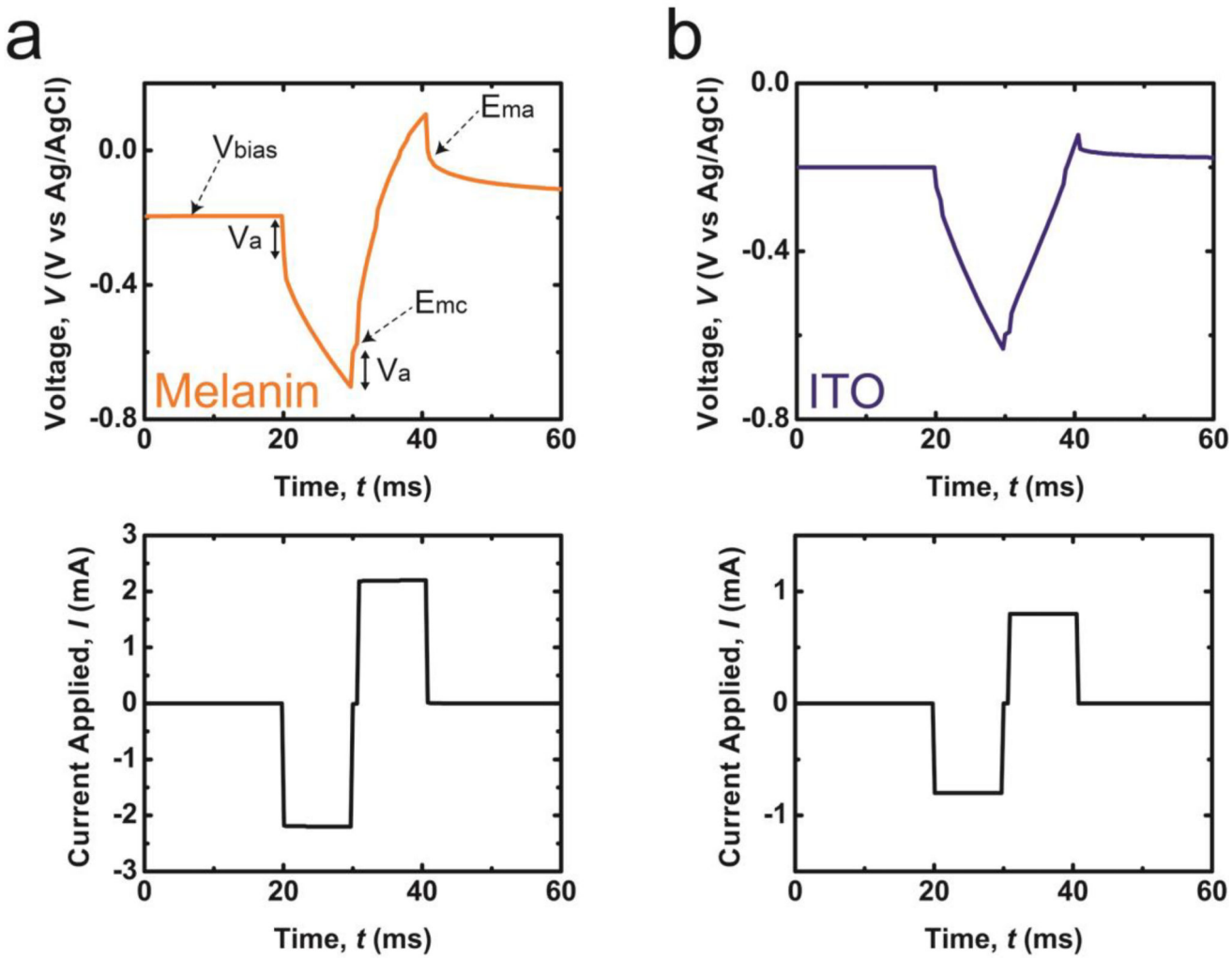

Figure 1.

Symmetric cathodal first waveform with a 10ms pulse-width and a 1ms dwell time, and corresponding voltage transient response ([Area] = 1 cm^2). V_{bias}: bias voltage versus Ag/AgCl; V_a: access voltage; E_{mc}: the most negative polarization; E_{ma}: the most positive polarization (a) ITO substrates coated with a 40nm thick film of polydopamine melanin (Melanin); (b) substrates composed of bare indium tin oxide (ITO).

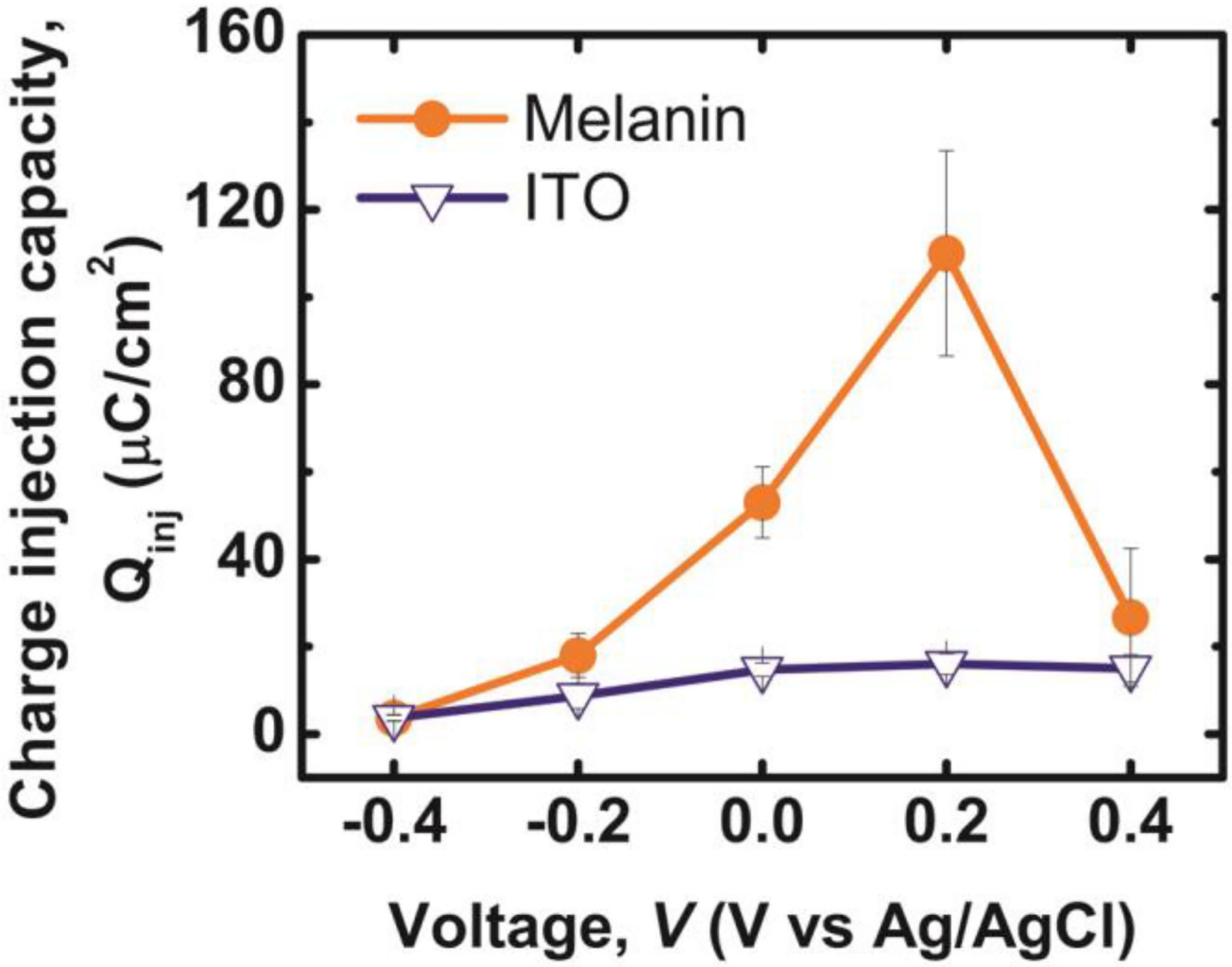

Figure 2.

Charge injection capacity (CIC) of as a function of the dc bias versus Ag/AgCl for the following samples: 40nm thick films of polydopamine melanin on indium tin oxide (Melanin); bare substrates composed of indium tin oxide (ITO).

Values are presented as mean ± stdev (n=3).

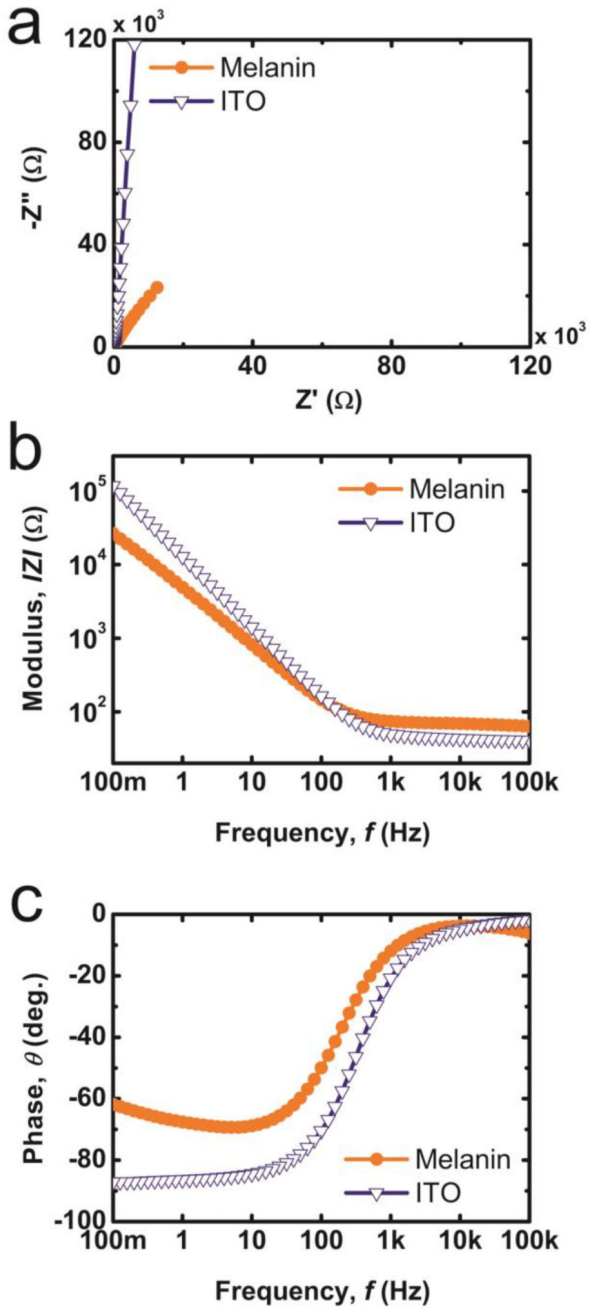

Figure 3.

Nyquist plots and bode plots from EIS measurements on a 40nm thick polydopamine melanin films coated on indium tin oxide (Melanin) and bare indium tin oxide (ITO) in the frequency range of 10^{-1}–10^{5}Hz at open circuit potential ([Area = 1cm^2). Representative graphs are shown including (a) a Nyquist plot, (b) /*Z*/ versus *f* (c) and phase versus *f*.

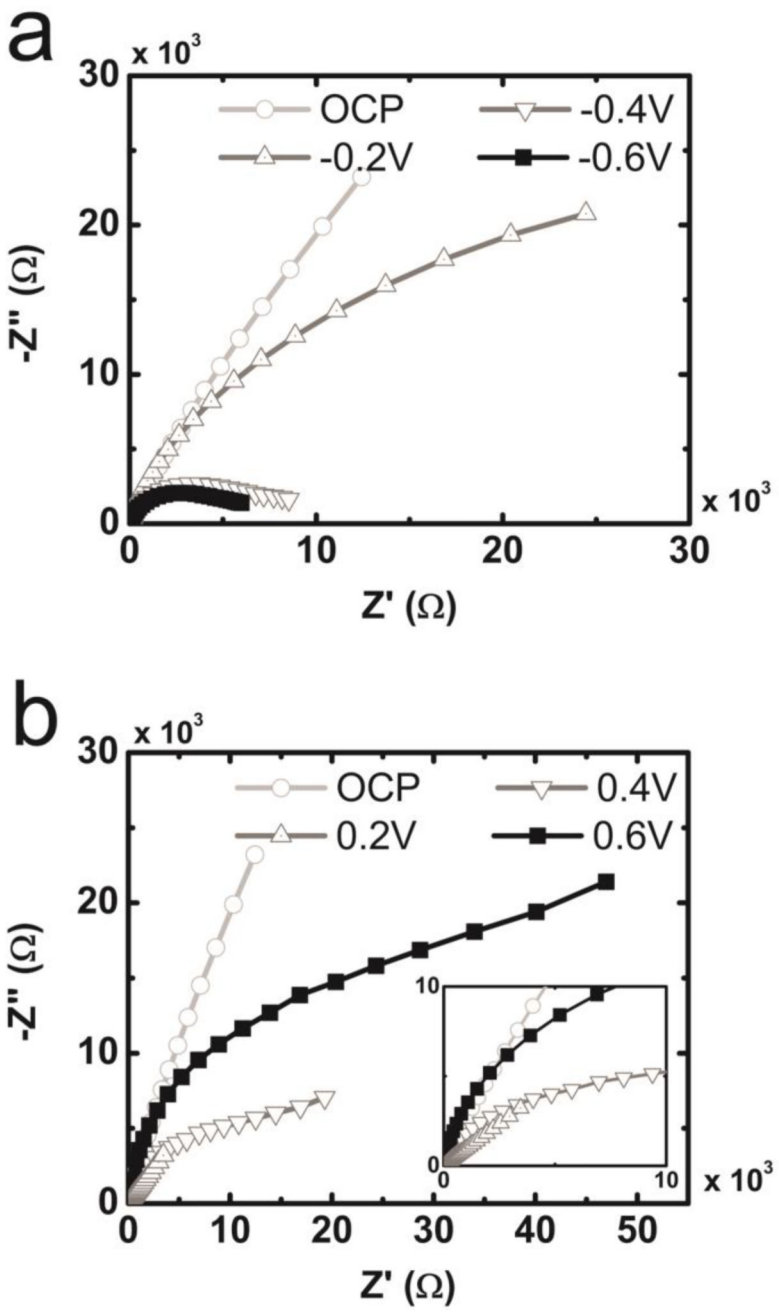

Figure 4.

Nyquist plots from EIS measurements on 40nm thick polydopamine melanin films coated on indium tin oxide in 0.01M PBS in the frequency range of $f = 10^{-1} – 10^{5}$ Hz, applying dc biases between −0.6V to 0.6V versus Ag/AgCl ([Area = 1cm^2).

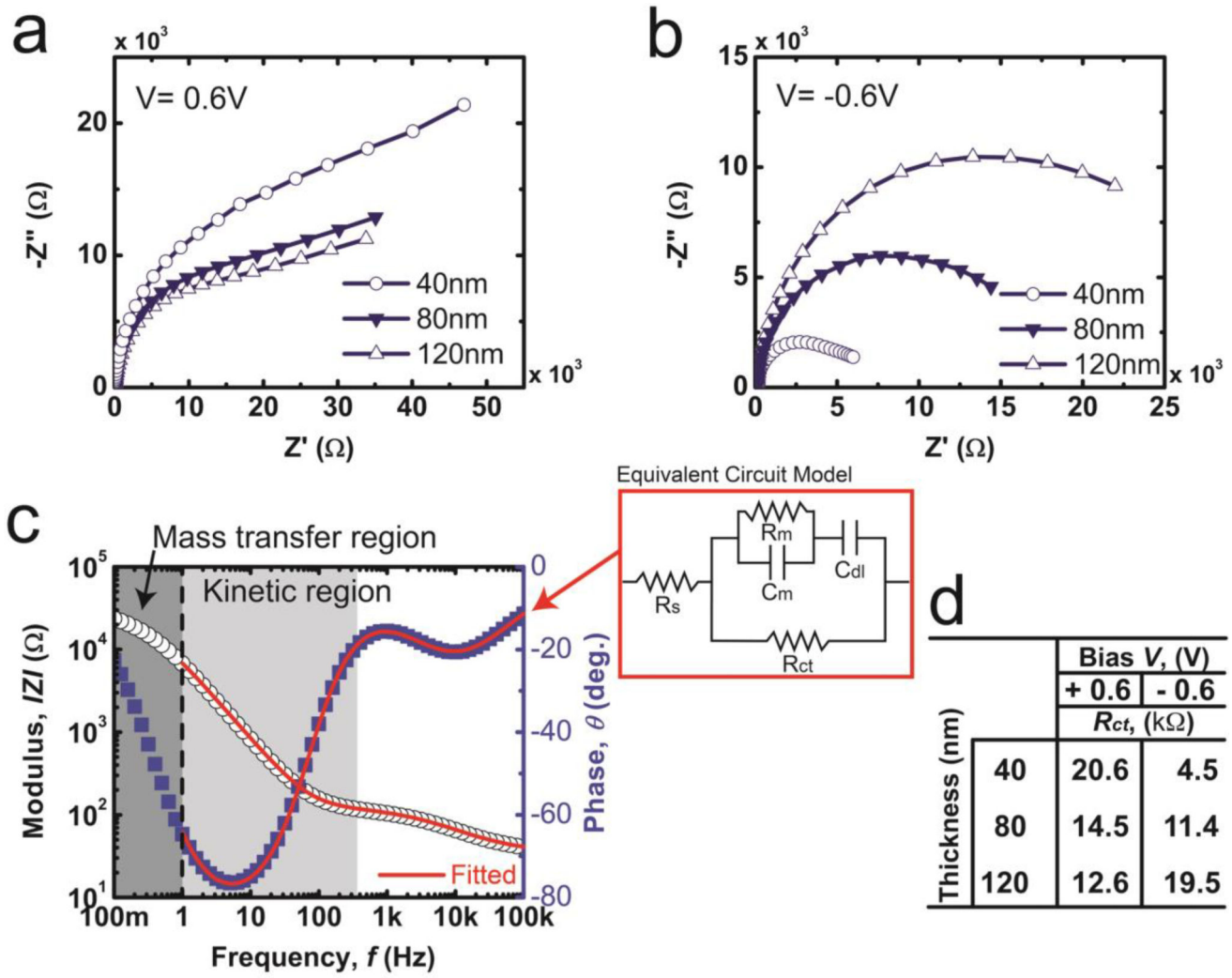

Figure 5.

Nyquist plots from EIS measurements on polydopamine melanin films of varying thicknesses coated on indium tin oxide substrates in 0.01M PBS in the frequency range of 10^{-1}–10^{5}Hz ([Area = 1cm^2). at (a) E_{dc} = 0.6V versus Ag/AgCl (b) E_{dc} = −0.6V versus Ag/AgCl (c) A representative results of the fit between experimental data and the model is shown for an ITO substrate with a PDM film 120nm in thickness at a dc bias of E_{dc} = −0.6V versus Ag/AgCl. The data is fit using a modified Randles circuit model with the following parameters: solution resistance (R_s); film capacitance contribution of the constant phase element (C_m, CPE); out of plane resistance of the film (R_m); double layer capacitance contribution of the constant phase element (C_{dl}, CPE); charge transfer resistance (R_{ct}). (d) The circuit diagram of the modified Randle's circuit model and a tabulation of extracted values of R_{ct} from this model.